Competition between ferromagnetism and antiferromagnetism: origin of large magnetoresistance in polycrystalline $SrRu_{1-x}Mn_xO_3$ ($0 \leq x \leq 1$)

2007 J. Phys.: Condens. Matter 19 266211

(http://iopscience.iop.org/0953-8984/19/26/266211)

IOP PUBLISHING JOURNAL OF PHYSICS: CONDENSED MATTER

J. Phys.: Condens. Matter **19** (2007) 266211 (15pp) doi:10.1088/0953-8984/19/26/266211

Competition between ferromagnetism and antiferromagnetism: origin of large magnetoresistance in polycrystalline $SrRu_{1-x}Mn_xO_3$ ($0 \leqslant x \leqslant 1$)

Xiao-Yu Zhang[1,2], Yajie Chen[3,4], Zhen-Ya Li[1], Carmine Vittoria[3] and Vincent G Harris[3]

[1] Department of Physics and Jiangsu Key Laboratory of Thin Films, Suzhou University, Suzhou 215006, People's Republic of China
[2] Laboratory of Solid State Microstructures, Nanjing University, Nanjing 218008, People's Republic of China
[3] Center for Microwave Magnetic Materials and Integrated Circuits, and the Department of Electrical and Computer Engineering, Northeastern University, Boston, MA 02115, USA

E-mail: y.chen@neu.edu

Received 23 February 2007, in final form 10 May 2007
Published 7 June 2007
Online at stacks.iop.org/JPhysCM/19/266211

Abstract

Polycrystalline $SrRu_{1-x}Mn_xO_3$ ($0 \leqslant x \leqslant 1$) perovskite oxides have been prepared by a conventional solid-state reaction technique. Magnetic and magnetotransport properties are measured using a superconducting quantum interference device (SQUID, Quantum Design MPMS) over a temperature range of 4–300 K. The substitution of Mn ions for Ru drives the system from a ferromagnetic state, $SrRuO_3$, to an antiferromagnetic state, $SrMnO_3$, which is basically similar to observations in single-crystal $SrRu_{1-x}Mn_xO_3$ (Cao *et al* 2005 *Phys. Rev.* B **71** 035104). However, the measurement of dc magnetization and ac susceptibility indicates that magnetic phase transition with x is more complicated and pronounced than those in single crystals. The phase transition process as temperature is reduced covers paramagnetism–antiferromagnetism (PM–AFM), paramagnetism–ferromagnetism (PM–FM) and ferromagnetism–cluster glass–spin glass (FM/CG/SG) etc. In particular, we observe a large low-temperature magnetoresistance (MR) of -41% for the sample $x = 0.55$, which is the largest MR measured in Mn-doped $SrRuO_3$. The experiment has verified that the large MR stems predominantly from a unique spin glass state in the polycrystalline alloy. These results substantiate that Ru-based oxides doped with 3d/4d transition metals have the potential for use in spintronics devices due to their adjustable phase transition, depending upon the level and nature of 3d/4d ion doping.

[4] Author to whom any correspondence should be addressed.

1. Introduction

Transition metal perovskite oxides are of lasting interest due to unique physical phenomena (such as colossal magnetoresistance, percolation, phase separation etc) that result from highly correlated d-band electrons and strong electron–lattice coupling [1, 2]. The ruthenates, as a class of strongly correlated systems, have received much attention due to their 'poor' metallic conduction properties and itinerant ferromagnetism which arises from low-spin t_{2g}^4 electrons of Ru^{4+} [3, 4]. Nevertheless, stoichiometric $SrRuO_3$ is ferromagnetic with a Curie temperature, T_c, of ∼160 K and it has a saturation moment of $1.6\mu_B$/Ru [5]. Due to their metallic conductivity and ease of epitaxial growth on various perovskite substrates, the doped perovskite oxides are potentially useful as electrode materials for spintronics devices [6].

Due to the role of d electrons with t_{2g} and e_g characters, the substitution of 3d metal ions on the cation B-sites can effectively change the physical properties of $SrRuO_3$ material and make the doped $SrRuO_3$ more intriguing. Previous investigations have addressed many important observations, such as a metal–insulator transition, ferromagnetic insulator, antiferromagnetic insulator, etc in $SrRu_{1-x}M_xO_3$ ($M = Mg^{2+}, Zn^{2+}, Ni^{2+}, Cr^{3+}, Fe^{3+}, Mn^{4+}, Ti^{4+}$) polycrystalline materials with different doping levels of foreign elements [7–16]. The change in physical property may arise from the introduction of local lattice distortions and/or the band formation in which these doping elements participate. One of the most striking among those is the substitution of Mn for Ru in $SrRu_{1-x}M_xO_3$ oxide, in that the solid solution formed with $SrRuO_3$ and $SrMnO_3$ exhibits complicated magnetic phase transitions and an enhancement of magnetoresistance (MR) that may be related to a phase transition.

$SrRu_{1-x}Mn_xO_3$ polycrystalline materials present interesting phenomena, such as mixed valence of Mn^{3+}/Mn^{4+} and Ru^{4+}/Ru^{5+} redox pairs, short-range magnetic clusters, and enhanced MR effects, rather than single-crystal $SrRu_{1-x}Mn_xO_3$ [12]. Han *et al* [13] and Yokoyama *et al* [14] have demonstrated Mn/Ru electronic states and magnetic interaction in polycrystalline $SrRu_{1-x}Mn_xO_3$ by nuclear magnetic resonance and neutron diffraction measurements. They found that the magnetic phase exhibited a coexistence of ferromagnetic (FM) interaction between Mn ions and antiferromagnetic (AFM) coupling between Mn and Ru moments below the Curie temperature, which was somewhat different from the quantum critical point from FM to AFM transition in single-crystal samples. This discrepancy mainly resulted from the degree of magnetic interactions between Mn and Ru moments. Although the magnetoresistance of polycrystalline $SrRuO_3$ compacts may be enhanced by doping Mn [15, 16], the cause still remains controversial. Banerjee *et al* found that an enhanced MR for a $SrRu_{0.9}Mn_{0.1}O_3$ ($x = 0.1$) sample only appeared at a spin freezing temperature of 140 K (lower than the Curie temperature of 160 K) [15], whereas Sahu's experiment indicated that the enhancement of MR occurred at $x = 0.5$ near the Curie temperature due to a double exchange mechanism [16]. Therefore, the present work attempts to carry out a more profound and systematic investigation of the variation in magnetic phase transition, magnetic properties, and, in particular, magnetoresistance behaviour with the composition of polycrystalline $SrRu_{1-x}Mn_xO_3$ ($0 \leqslant x \leqslant 1$) compacts. These efforts will be helpful to straighten up the physical mechanisms of phase transitions and the origin of the large MR effect for the polycrystalline $SrRu_{1-x}Mn_xO_3$ materials.

2. Experiment

Polycrystalline $SrRu_{1-x}Mn_xO_3$ samples were prepared by a routine solid-state reaction process. High-purity $SrCO_3$, RuO_2 and MnO_2 powders were mixed with an agate mortar and pestle. The calcination of the initial mixture was performed at 700 °C for a short time (1 h) to

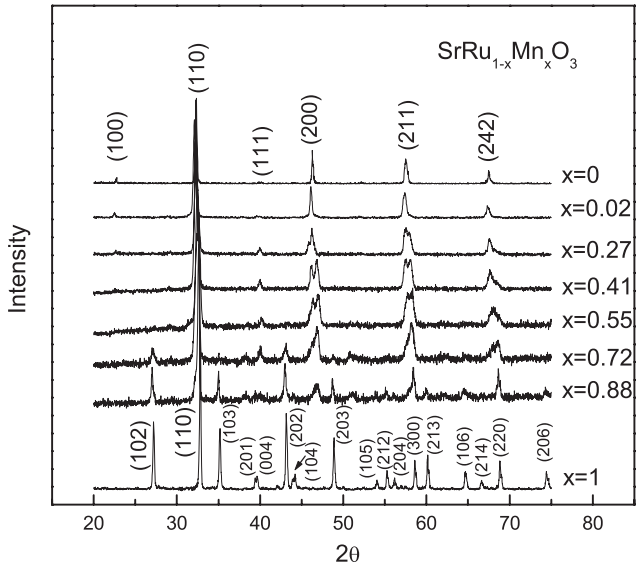

Figure 1. X-ray diffraction patterns for $SrRu_{1-x}Mn_xO_3$ samples recorded at room temperature.

minimize the loss of the Ru due to the volatility of RuO_2. The mixed powders were pressed into pellets and then fired in air for 96 h at a final sintering temperature of 1100 °C for the sample with $x = 0$ and 1150 °C for the samples with $x > 0$. During sintering, the $SrRu_{1-x}Mn_xO_3$ compacts were embedded in $SrRuO_3$ powder to stabilize the vapour pressure of the volatile Ru. After sintering, the surface layers of pellets were removed before further characterization.

Crystallography measurements on these samples were carried out using a Rigaku D/Max 2500C x-ray diffractometer (XRD) with Cu Kα radiation. The chemical composition of the samples was determined by energy dispersive x-ray spectroscopy (EDXS). The magnetic properties, including zero field cooled (ZFC) and field cooled (FC) magnetization, were measured using a superconducting quantum interference device (SQUID) (Quantum Design MPMS). Measurement of the ac susceptibility, χ, was performed at $h_{ac} = 10$ Oe and $f = 10$–1000 Hz over a temperature range from 4 to 300 K using a Quantum Design physical property measurement system (PPMS). The chemical valence state of ions was characterized using a PHI-550 x-ray photoelectron spectrometer (XPS). The resistivity and magnetoresistance were measured for samples (10 mm × 2 mm × 1 mm) in a four-probe configuration.

3. Results and discussion

The XRD patterns of the $SrRu_{1-x}Mn_xO_3$ samples ($0 \leqslant x \leqslant 1$) are displayed in figure 1. These patterns show that the compounds are highly crystalline and homogenous, and no second phase is found. With Mn doping, splitting of the (200) and (211) peaks are observed for samples with $x = 0.27$, 0.41 and 0.55. The splitting phenomenon is attributed to the distortion of the orthorhombic structure and redox mechanism [15, 16]. Although two small peaks at $2\theta = 38.3$ and 51.3° are found in Mn-rich compounds with $x = 0.72$ and 0.88, two peaks are verified to come from the γ-$SrMnO_3$ phase, which has a larger c-axis than that of $SrMnO_3$ (orthorhombic symmetry) due to the lattice deformation induced by the different ionic radii of Ru^{4+}(0.63 Å) and Mn^{4+}(0.52 Å). To clarify uniformity for these samples, a scanning electron microscope (SEM) and energy dispersive x-ray analysis (EDX) were used to determine the ratio of Ru to

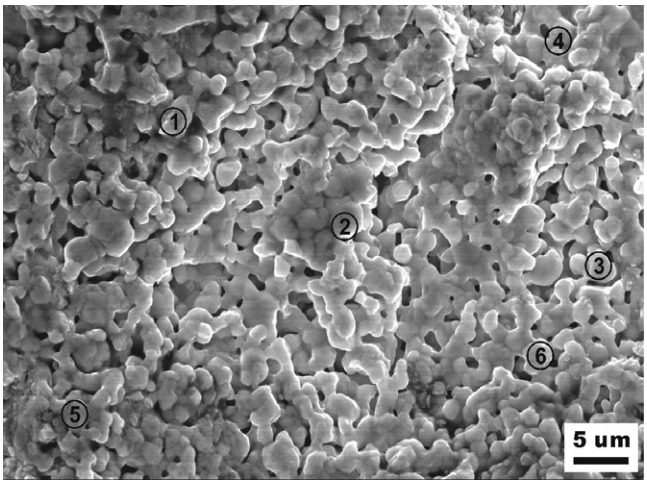

Figure 2. SEM micrograph for $SrRu_{1-x}Mn_xO_3$ ($x = 0.55$) sample. The six circles represent areas of EDXS spot analysis.

Table 1. Atom number of Ru and Mn at different spots.

Position	Ru (atom mol^{-1})	Mn (atom mol^{-1})
Entire scanned area	0.450	0.550
Spot 1	0.445	0.555
Spot 2	0.442	0.558
Spot 3	0.464	0.536
Spot 4	0.461	0.539
Spot 5	0.449	0.551
Spot 6	0.454	0.546

Mn atoms at different spots. For a typical sample with $x = 0.55$, the EDS results are listed in table 1, corresponding to the six spots that were probed in figure 2. Clearly, either the Mn atom number or the Ru atom number is nearly the same at every spot, and very close to the measured value over the entire scale of the SEM image. Thus, the deviation in metallic atom number is only about 0.55% at different spots, which provides direct evidence for the assumption of an homogeneous system.

Figure 3 shows the dc magnetization as a function of temperature for the $SrRu_{1-x}Mn_xO_3$ samples ($0 \leqslant x \leqslant 0.72$). The $M(T)$ of the samples is measured at a magnetic field of 10 kOe while warming after a field cooled process ($H = 10$ kOe). Although the parent compound $SrRuO_3$ has a ferromagnetic Curie temperature of T_c, ~160.5 K, the Curie temperature for the Mn-doped solid solution reduces gradually with Mn doping. Apparently, the Curie temperature T_c decreases with increasing Mn concentration as well, which is in good agreement with observations made in single-crystal $SrRu_{1-x}Mn_xO_3$ [12]. For $x = 0.55$, T_c drops to 94 K, whereas for the sample with $x = 0.72$ the magnetization is almost linearly dependent on temperature. This implies that the composition has a marked effect on ferromagnetism. The change in the magnetic state is comparable to the measurement of isothermal magnetization M, as shown in figure 4. The magnetization M for $x = 0$ and 0.05 displays a field dependence that is similar to typical ferromagnets. However, a linear field dependence of magnetization for $x \geqslant 0.72$ is predominantly ascribed to antiferromagnetism.

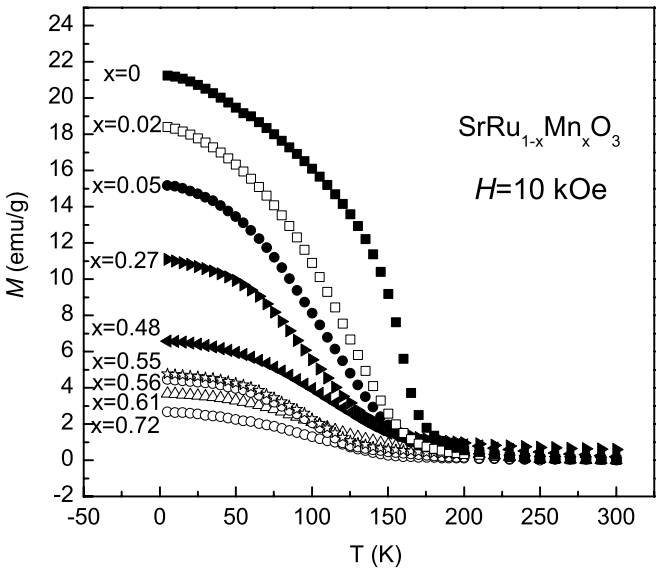

Figure 3. dc magnetization as a function of temperature for different compositions. (Field cooling at 10 kOe.)

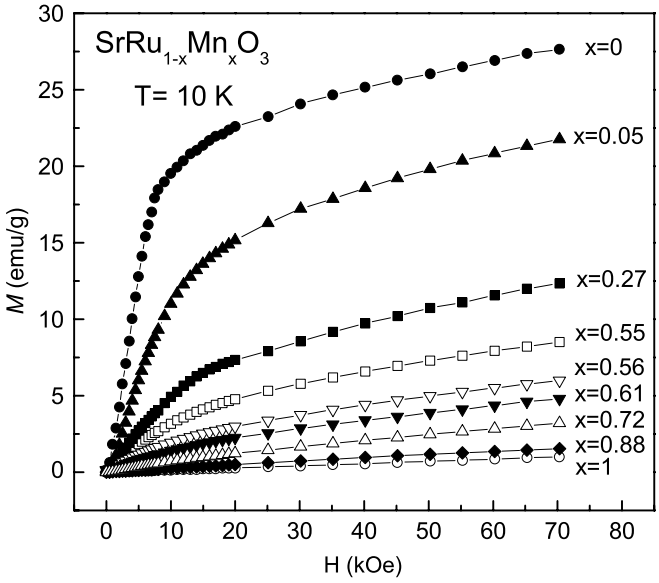

Figure 4. Isothermal magnetization M as a function of applied field at $T = 10$ K for different Mn concentrations.

In addition, the ferromagnetism is retained in samples until Mn doping reaches 0.61. We can estimate the effective magnetic moment p_{eff} by fitting M–T curves according to the Curie–Weiss law $\chi = \chi_0 + C/(T - \theta)$. Here, χ_0 is a temperature-independent term, and C and θ are the Curie constant and the Curie–Weiss temperature, respectively. The susceptibility χ is defined as M/H and the fitting range is from 240 to 300 K (in the paramagnetic region). The

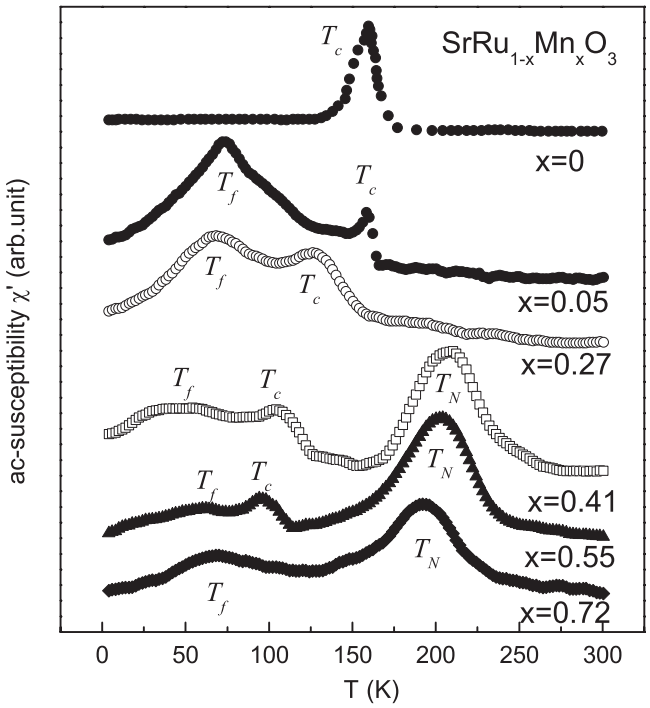

Figure 5. Temperature dependence of the real part of ac susceptibility χ' for $SrRu_{1-x}Mn_xO_3$ ($x = 0$, 0.05, 0.27, 0.55 and 0.72).

value of p_{eff} can be obtained from

$$C = N_{\text{A}} p_{\text{eff}}^2 \mu_{\text{B}} / 3k_{\text{B}}, \tag{1}$$

where N_{A} is Avogadro's number, μ_{B} is the Bohr magneton, and k_{B} is the Boltzmann constant. For comparison, however, a theoretical prediction, p_{theory}, of the effective magnetic moment can be calculated from:

$$p_{\text{theory}}^2 = (g\sqrt{S(S+1)})^2 = g^2[(1-x)S_{\text{Ru}^{4+}}(S_{\text{Ru}^{4+}}+1) + xS_{\text{Mn}^{4+}}(S_{\text{Mn}^{4+}}+1)], \tag{2}$$

where x is the Mn doping concentration and $g(=2)$ is the Lande factor if only considering the spin $S = 1$ for Ru^{4+} and the spin $S = 3/2$ for Mn^{4+}. The results of this analysis are presented in table 2. The p_{eff} value for $x = 0$ is approximately equal to the predicted p_{theory}. Thus, it is reasonable to assume that the valence state of Ru in $SrRuO_3$ is basically tetravalent. However, it is noted that the values of p_{eff} are larger than p_{theory} for the samples where $x \geqslant 0.05$. The results are not found in single-crystal $SrRu_{1-x}Mn_xO_3$, where the p_{eff} is close to the expected moment for tetravalent Ru and Mn ions. Therefore, it can be deduced that the increased p_{eff} is attributed to Mn^{3+} ($S = 2$) and Ru^{5+} ($S = 3/2$) ions with high spin, i.e. Mn^{3+}/Mn^{4+} and Ru^{4+}/Ru^{5+} may appear in the samples simultaneously. The assumption has been verified by x-ray photoelectron spectroscopy measurements discussed below.

Figure 5 displays the temperature dependence of the real part of the ac susceptibility, χ', for the samples $x = 0$, 0.05, 0.27, 0.41, 0.55 and 0.72. The χ'–T curves clearly depict magnetic phase transitions with variation of Mn concentration. For $x = 0$, a sharp peak in χ' is observed at a Curie temperature T_{c} of 160 K, which is consistent with the M–T measurement. Meanwhile, the sharp peak at T_{c} is related to the high magnetic anisotropy characteristic of

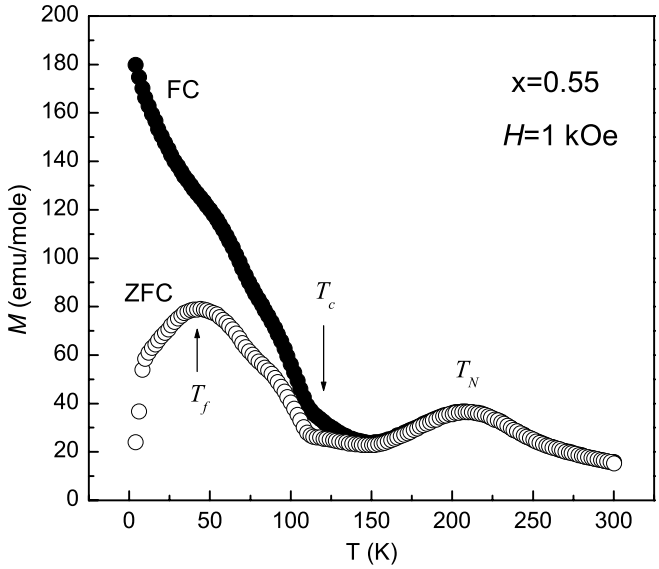

Figure 6. Field cooling (FC) and zero field cooling (ZFC) magnetization as a function of temperature for sample $x = 0.55$.

Table 2. Magnetic parameters of the $SrRu_{1-x}Mn_xO_3$ compounds deduced by fitting the temperature-dependent magnetization.

Composition, x	T_c (K)	C (emu K mol^{-1} Oe^{-1})	p_{eff} (μ_B)	p_{theory} (μ_B)
0	160	1.00	2.81	2.83
0.05	159	1.07	2.91	2.89
0.27	126	1.35	3.27	3.14
0.48	110	1.53	3.48	3.37
0.55	94	1.68	3.65	3.44
0.56	91	1.72	3.69	3.45
0.61	105	1.59	3.55	3.50

$SrRuO_3$ [5]. With an increase in the amount of Mn, the samples $x = 0.05$ and 0.27 exhibit two peaks in χ'. One corresponds to T_c, whereas another is associated with the spin freezing temperature T_f. Furthermore, the curve of χ'–T for the samples $x = 0.41$ and 0.55 shows three peaks, which arise from T_c, T_f and an antiferromagnetic Néel temperature T_N, respectively. The experimental results indicate that ferromagnetic phases, antiferromagnetic phases and weak magnetic clusters coexist in the samples studied. When Mn doping is beyond $x = 0.72$, we can see only two peaks corresponding to T_f and T_N, respectively. The disappearance of T_c is related to a weakened ferromagnetism in the high Mn-doped samples. This is in accordance with the dc magnetization data of figure 3. The characteristic temperatures (T_c, T_f and T_N) are also in agreement with field cooled (FC) and zero field cooled (ZFC) magnetization, as shown in figure 6. Here, the FC and ZFC curves for the $x = 0.55$ sample are measured at a small magnetic field of 1 kOe. At $T = 55$ K, ZFC exhibits a decrease in magnetization with reducing temperature, which is considered to be a typical characteristic of spin glass behaviour [17]. However, the M–T curves between FC and ZFC magnetizations display a bifurcation close to T_c, indicating the lack of a true long-range ordering. This is a characteristic of a cluster glass

(CG) [18, 19]. Clearly, a broad peak appears at 210 K in both the FC and ZFC curves. This is a transition from antiferromagnetism to paramagnetism, i.e. the Néel temperature T_N.

To verify the existence of the spin glass transition at low temperatures, we perform measurement of the frequency dependence of ac susceptibility for the sample $x = 0.55$ from 4 to 267 K. In view of the magnetic structure, however, a spin glass usually exhibits frozen magnetic moments below the freezing temperature T_f, and a lack of periodic long-range magnetic order, whereas a cluster glass can be considered to be a modified version of the spin glass system and a set of clusters, formed due to short-range ordering at temperatures near the Curie-like temperature T_c. The ac susceptibility χ' curves are separated in the SG/CG region below T_c, clearly demonstrating the dynamic effects in association with the magnetic structure. Namely, the frequency dependence of χ' is exhibited in the temperature range 40–110 K, where the system experiences spin glass, cluster glass and ferromagnetic phase transitions. It is worth mentioning that the peaks at T_f are frequency dependent, and they shift toward higher temperature as the frequency f increases from 10 to 1000 Hz. Obviously, this strongly supports the existence of a spin glass in the material. Moreover, the spin glass changes to a cluster glass above T_f, which makes the sample retain the frequency dependence of ac susceptibility over a wide temperature range, but the peaks at T_c are frequency independent. Furthermore, in the paramagnetic region ($T > 220$ K) we are able to observe an insensitive frequency dependence of ac susceptibility. As shown in the inset of figure 7, more importantly, T_f is linear in the logarithm of frequency with a slope p:

$$p = \Delta T_f/(T_f \Delta \log_{10} f). \tag{3}$$

Thus, we can obtain $p = 0.0225$, a typical value for canonical spin glass systems, in which p ranges from 0.0045 to 0.28 [20]. The estimate is further helpful to having a good understanding of the spin glass transition for the present sample. Such spin glass behaviour is also observed in other samples ($0.05 \leqslant x \leqslant 0.61$) in the present experiment.

By combining static and dynamic magnetization measurements, one may construct a magnetic phase diagram for the polycrystalline $SrRu_{1-x}Mn_xO_3$ samples. This is presented as figure 8. The phase boundary of ferromagnetic (FM), antiferromagnetic (AFM), cluster glass (CG), and spin glass (SG) states is determined by the characteristic temperature dependence of magnetization. The PM–FM and PM–CG transitions are denoted by T_c, whereas T_f and T_N represent the CG/SG and PM/AFM transitions, respectively [9, 17]. It is clearly seen that low-level substitutions of Mn for itinerant Ru gives rise to a marked change in the magnetic properties. As illustrated in the phase diagram, the magnetic phase not only transfers from the FM to the AFM state, but also undergoes a spin glass or cluster glass transition in the polycrystalline $SrRu_{1-x}Mn_xO_3$ system. In comparison, single-crystal Mn-doped samples only exhibit a simple phase transition of FM–AFM–PM [12]. In our experiment, the Mn^{4+} ion doping yields an antiferromagnetic superexchange interaction via Mn^{4+}–O–Mn^{4+}. The antiferromagnetic arrangement of the spins certainly competes with a ferromagnetic order, such as itinerant ferromagnetic $SrRuO_3$, ferromagnetic double exchange (DE) interaction through Mn^{3+}–O–Mn^{4+} and/or Mn^{3+}–O–Ru^{5+}, and ferromagnetic superexchange interaction through Mn–Ru. Actually, FM and AFM clusters randomly emerge with a short-range ordering. The randomness of the signs of neighbouring coupling (FM or AFM) is one of the most important prerequisites for the formation of the magnetically inhomogeneous state. As a result of the competition, it is inevitable for the materials to exhibit the short-range magnetic clusters or magnetic inhomogeneity state [21–23], which may result in a complicated magnetic phase diagram.

In order to verify the existence of mixed valence in the samples, x-ray photoelectron spectroscopy (XPS) is used to characterize the oxidation state of Mn and Ru ions. We measured

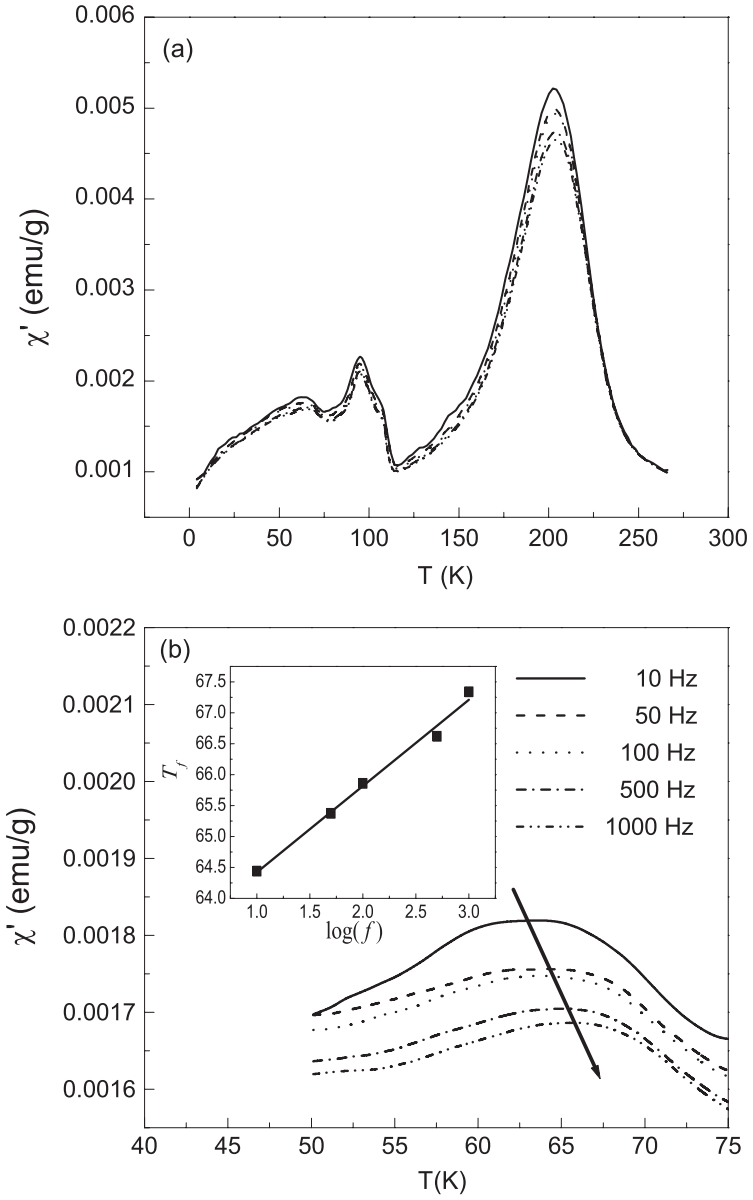

Figure 7. (a) Real part χ' of ac susceptibility versus temperature at different frequencies for sample $x = 0.55$. (b) ac susceptibility χ' as a function of temperature over the amplified range 50–75 K. The inset shows the variation in the temperature of the χ' peak with frequencies ranging from 10 to 1000 Hz.

XPS for the sample with $x = 0.55$, sample Mn_2O_3 (Mn^{3+} ion), sample MnO_2 (Mn^{4+} ion), and sample RuO_2 (Ru^{4+} ion), as shown in figure 9. All XPS measurements were performed with a calibration of the C 1s core-level peak of 284.6 eV. Due to an overlap of the peaks of C 1s and Ru $3d_{3/2}$, no discernable feature of a C 1s core-level peak can be seen at 284.6 eV. Moreover, it is worth noting that the measured values for the known oxides (RuO_2, MnO_2 and Mn_2O_3) are in good agreement with [24]. That is, the measured binding energies are 280.9 and 285.1 eV

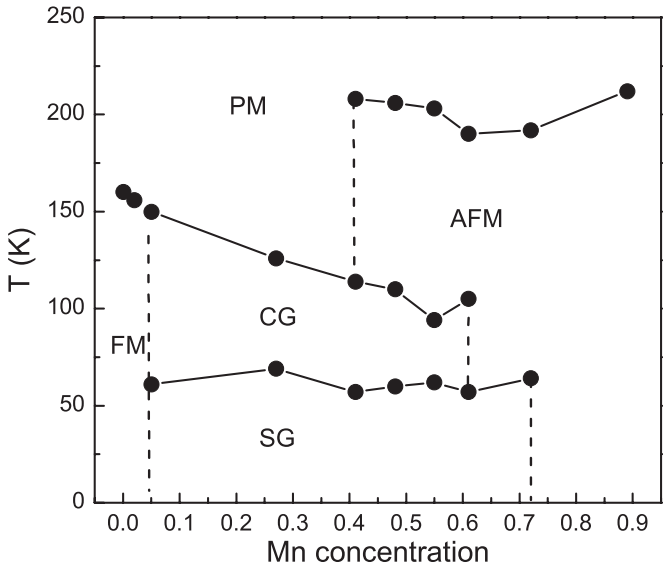

Figure 8. Magnetic phase diagram for polycrystalline $SrRu_{1-x}Mn_xO_3$: FM = ferromagnetic; PM = paramagnetic; SG = spin glass; CG = cluster glass; AFM = antiferromagnetic.

for Ru $3d_{5/2}$ and Ru $3d_{3/2}$, as well as 642.3 and 641.5 eV for Mn^{4+} $2p_{3/2}$ and Mn^{3+} $2p_{3/2}$, respectively (see figure 9(a)). Therefore, the measurements are believable, which will allow us to discuss them profoundly below.

The sample with $x = 0.55$ has an Mn $2p_{3/2}$ binding energy of 642.0 eV, indicating that the Mn ions exist as Mn^{3+} and Mn^{4+} ions at the same time. In figure 9(b), the binding energy of Ru $3d_{5/2}$ for $x = 0.55$ is 281.8 eV, which also deviated from the reported values 280.9 eV for RuO_2 and 282.5 eV for RuO_3 [25, 26]. It is a fact that the appearance of $Mn^{4+} \rightarrow Mn^{3+}$ and $Ru^{4+} \rightarrow Ru^{5+}$ is spontaneous and inevitable for charge balance of the valence states. These results support our assumption that high-spin Mn^{3+} and Ru^{5+} ions are responsible for the large effective magnetic moment, p_{eff}, in the samples.

Figure 10(a) shows the magnetoresistance (MR) ratio as a function of magnetic field up to 70 kOe at $T = 10$ K for different Mn substitutions. The MR ratio is defined as $\mathrm{MR} = [\rho(H) - \rho(0)]/\rho(0)$, where $\rho(0)$ and $\rho(H)$ are the resistivities at zero field and an applied field, respectively. The negative MR ratio is only -6% for $SrRuO_3$, but increases significantly for Mn-doped samples. It is worth noting that the samples ($x = 0.55$) exhibits a large MR of -41%. Subsequently, the MR will reduce with increasing x. The variation in MR with Mn concentration is presented in figure 10(b). Such an observation of large MR in the system is impressive. Therefore, the samples are reproduced three times for each composition. The experimental results indicate that all of the samples ($x = 0.55$) for different lots yield MRs of -39.9%, -41.1% and -40.8% at 10 K, respectively. This manifests that the results are reproducible. We believe that the large MR is certainly associated with the spin glass phase at low temperature [17]. However, a peak in the MR (-35%) can be seen at $\sim$95 K (T_c) in the MR versus T curve, as shown in figure 11(a). Therefore, the significant magnetotransport properties allow us to reveal the origin of MR in polycrystalline $SrRu_{1-x}Mn_xO_3$.

It must be emphasized that the MR at 10 K is not only larger than that at T_c, but also varies linearly with an external magnetic field. This linear dependence reveals that MR is associated with field-induced magnetization. In order to investigate the correlation between

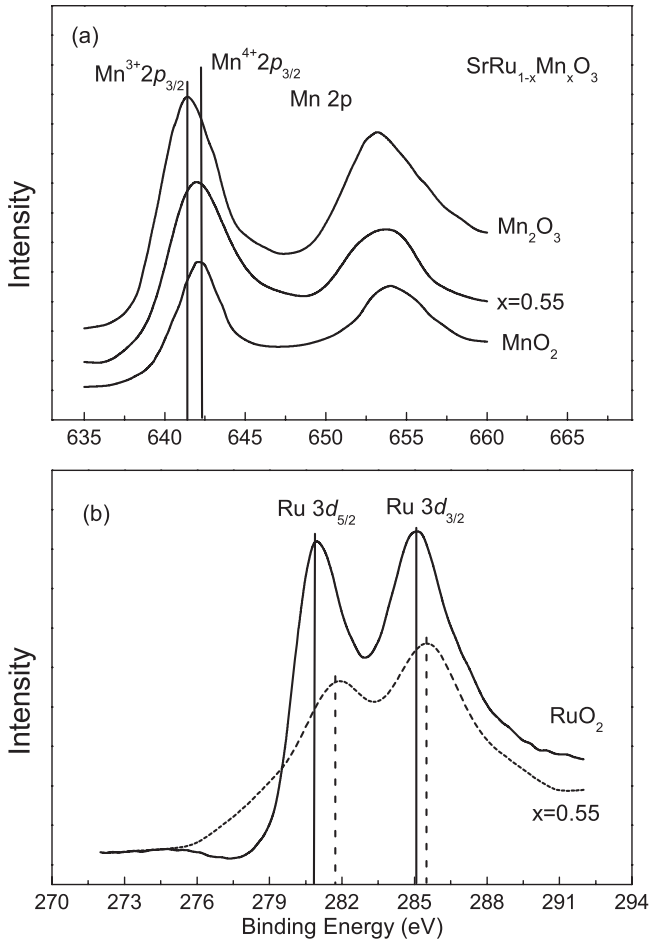

Figure 9. (a) XPS for Mn_2O_3, MnO_2 and the $SrRu_{0.45}Mn_{0.55}O_3$ sample. (b) Comparison of XPS between RuO_2 and $SrRu_{0.45}Mn_{0.55}O_3$.

MR and magnetization, we plotted the MR as a function of M^2 at a temperature of 10 K, as shown in figure 12. The plots are inspected by cross-plotting the MR(H) and $M(H)$ data in figures 10(a) and (c). Clearly, MR shows a good linear dependence with M^2 for these samples with large MR (-22% to -41%; $x = 0.48$–0.61). In contrast, the low Mn-doped samples ($x \leqslant 0.27$) only have a weak and nonlinear dependence with M^2. These observations indicate that the large MR is strongly related to the field-induced magnetization. Meanwhile, the inset of figure 12 presents the rapid increase in the average slope $MR_{7\ T}/(M_{7\ T})^2$ with composition for $x > 0.27$. This further supports that the frozen magnetization in spin glass predominantly contributes to the MR at low temperatures. In polycrystalline manganites, Hwang *et al* point out that the low-field MR is attributed to spin-polarized inter-grain tunnelling, and high-field MR arises from suppression of the intra-grain spin fluctuation [27]. In this experiment, frozen spin clusters become larger with a decrease in temperature. When a large external field is used to align these spin clusters, the magnetic disorder reduces and ferromagnetism arises, as shown in figure 10(c). This in turn suppresses the spatial spin fluctuation and favours charge delocalization. The process results in a large MR at low temperature. On the other hand, it is

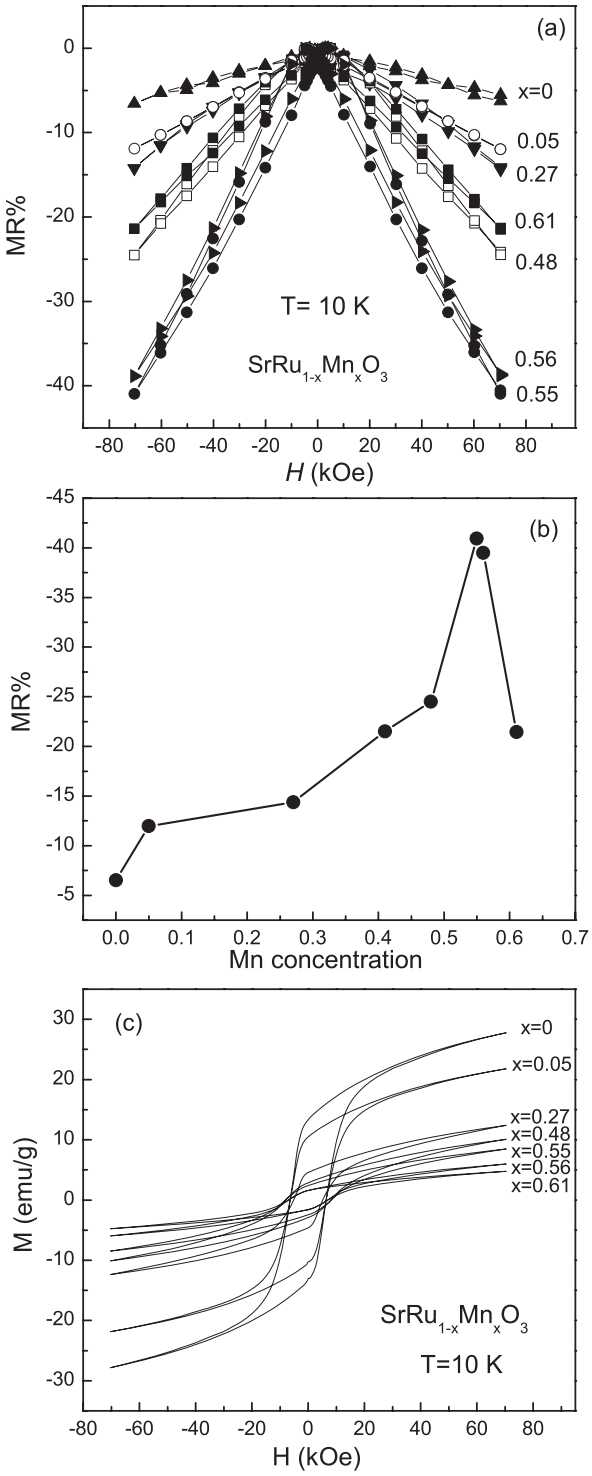

Figure 10. (a) Field dependence of magnetoresistance (MR) at 10 K for $SrRu_{1-x}Mn_xO_3$ samples. (b) The MR ratio as a function of Mn concentration at $T = 10$ K and $H = 70$ kOe. (c) Hysteresis loops at 10 K for $SrRu_{1-x}Mn_xO_3$ samples.

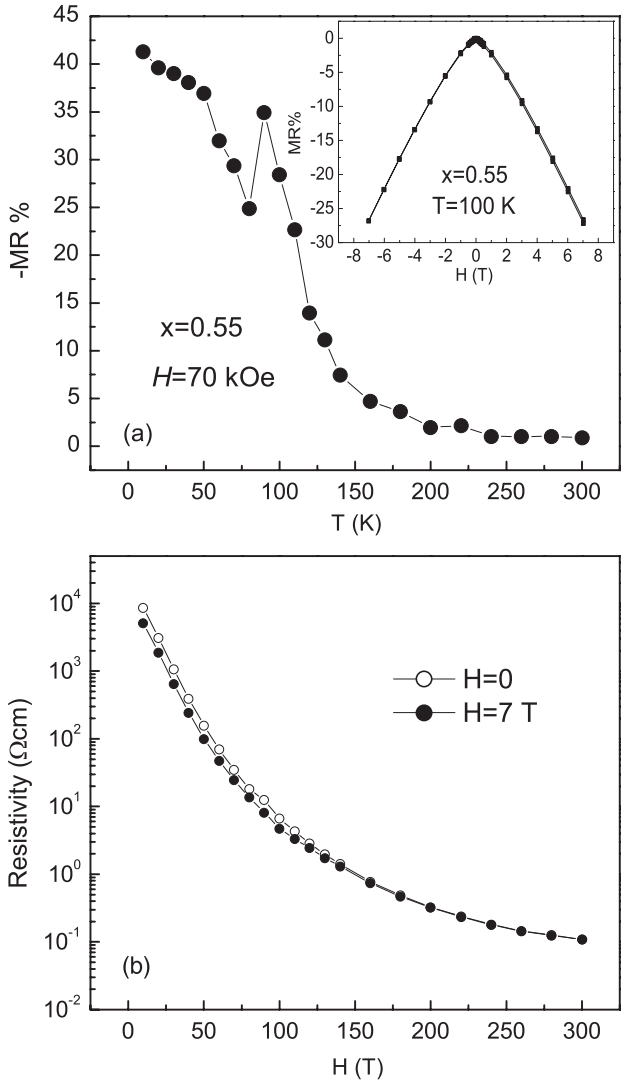

Figure 11. (a) Temperature dependence of magnetoresistance (MR) for the sample with $x = 0.55$ at an applied field of 70 kOe. The inset shows the field dependence of magnetoresistance at 100 K for the sample with $x = 0.55$. (b) Resistivity as a function of temperature at $H = 0$ and 7 T for the sample with $x = 0.55$.

found that a large MR is still linear with the magnetic field near T_c where the cluster glass exists, as shown in the inset of figure 11. The resistivity for $x = 0.55$ is small, and is 6.6 Ω cm at 100 K in figure 11(b). Therefore, the enhanced MR at T_c may result from the fact that the spin clusters are aligned under a high external field, giving rise to a decrease in the spin fluctuation and spin-dependent scattering, and hence the MR. An investigation on $Re_{1-x}AE_xMn_{1-y}T_yO_3$ indicates that the MR is still large due to the contribution of spin clusters, although the samples are either semiconducting or insulating in electrical transport (e.g. $La_{0.67}Sr_{0.33}Mn_{1-x}Ni_xO_3$) [9, 28, 29]. Furthermore, the magnetic inhomogeneity state possibly gives rise to the large MR due to the change in relative volumes of minority and majority phases with different conductivity at external magnetic field [21–23].

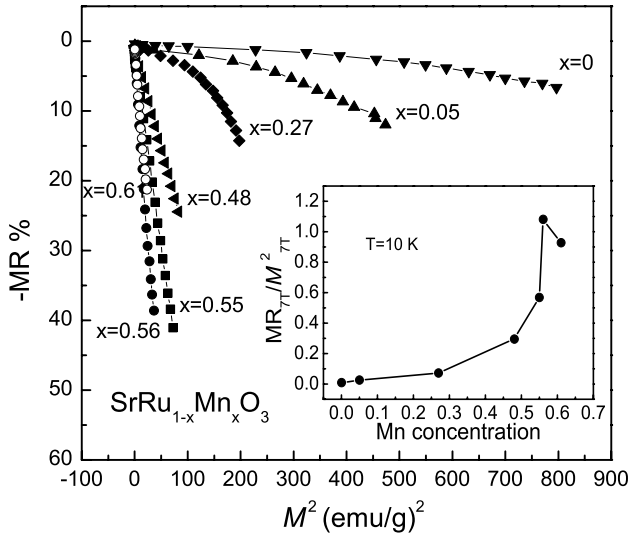

Figure 12. Variation in MR with M^2 at an applied field of 70 kOe and $T = 10$ K for the $SrRu_{1-x}Mn_xO_3$ samples. The inset presents the compositional dependence of $MR_{7\,T}/(M_{7\,T})^2$ on Mn concentration at 10 K.

The Mn substitution leads to a phase transition from the ferromagnetic state to the antiferromagnetic state, and the spin glass/cluster glass phases are verified over a wide range of Mn concentration. These weak magnetic clusters will grow larger with Mn doping. Therefore, a significant MR effect is usually exhibited at high Mn concentrations. It is noteworthy that large MR occurs not only at low temperature but also near T_c. However, in the antiferromagnetic region ∼200 K, the MR is actually very small, ∼1% at 7 T.

4. Conclusions

In conclusion, we have addressed the effect of Mn doping on magnetic and transport properties for the 3d/4d transition metal oxide $SrRu_{1-x}Mn_xO_3$. Unlike single-crystal materials, this work presents the rich interactions of magnetic phase transitions including itinerant ferromagnetism, antiferromagnetism and spin glass in polycrystalline $SrRu_{1-x}Mn_xO_3$. The spin glass state arising from the competition between ferromagnetism and antiferromagnetism gives rise to a large magnetoresistance of -41% for the sample with $x = 0.55$. In addition, we also observe a peak of MR (-35%) near the Curie temperature, which results from the decrease in the spin fluctuation and the spin-dependent scattering. Therefore, we believe that a weak short-range magnetic state and magnetic inhomogeneity in polycrystalline materials plays an important role in the enhancement of magnetoresistance. The experimental results are helpful in understanding the physical mechanisms contributing to the magnetotransport properties in 3d/4d transition metal doped perovskite oxides.

Acknowledgments

This work was supported in part by the National Natural Science Foundation of China under grant number 10474069, as well as by the US Defense Advanced Research Projects Agency (DARPA) under grant number HR0011-05-1-0011 and the US Office of Naval Research (ONR)

under grant number N00014-05-10349. X Y Zhang would like to thank Ms Liya Lü for the SQUID measurements in the National Laboratory of Solid State Microstructures at Nanjing University, China.

References

[1] Moreo A, Yunoki S and Dagotto E 1999 *Science* **283** 2034
[2] Tokura Y 2000 *Colossal Magnetoresistive Oxides* (New York: Gordon and Breach)
[3] Mazin I I and Singh D J 1997 *Phys. Rev.* B **56** 2556
[4] Klein L, Dodge J S, Ahn C H, Reiner J W, Mieville L, Geballe T H, Beasley M R and Kapitulnik A 1996 *J. Phys.: Condens. Matter* **8** 10111
[5] Cao G, McCall S, Shepard M, Crow J E and Guertin R P 1997 *Phys. Rev.* B **56** 321
[6] Eom C B *et al* 1992 *Science* **258** 1766
[7] Crandles D A, Mehdi M Y and Razavi F S 2006 *J. Phys. D: Appl. Phys.* **39** 6
[8] Williams A J, Gillies A, Attfield J P, Heymann G, Huppertz H, Martínez-Lope M J and Alonso J A 2006 *Phys. Rev.* B **73** 104409
[9] Mamchik A and Chen I-W 2004 *Phys. Rev.* B **70** 104409
[10] Kim K W, Lee J S, Noh T W, Lee S R and Char K 2005 *Phys. Rev.* B **71** 125104
[11] Pi L, Maignan A, Retoux R and Raveau B 2002 *J. Phys.: Condens. Matter* **14** 7391
[12] Cao G, Chikara S, Lin X N, Elhami E, Durairaj V and Schlottmann P 2005 *Phys. Rev.* B **71** 035104
[13] Han Z H, Budnick J I, Hines W A, Dabrowski B and Maxwell T 2006 *Appl. Phys. Lett.* **89** 102501
[14] Yokoyama M, Satoh C, Saitou A, Kawanaka H, Bando H, Ohoyama K and Nishihara Y 2005 *J. Phys. Soc. Japan* **74** 1706
[15] Banerjee G N, Bhowmik R N and Ranganathan R 2001 *J. Phys.: Condens. Matter* **13** 9481
[16] Sahu R K, Hu Z, Rao M L, Manoharan S S, Schmidt T, Richter B, Knupfer M, Golden M, Fink J and Schneider C M 2002 *Phys. Rev.* B **66** 144415
[17] Cai J W, Wang C, Shen B G, Zhao J G and Zhan W S 1997 *Appl. Phys. Lett.* **71** 1727
[18] Douglas D S and Leighton C 2004 *Phys. Rev.* B **70** 214414
[19] Karmakar S *et al* 2006 *Phys. Rev.* B **74** 104407
[20] Mydosh J A 1993 *Spin Glass: An Experimental Introduction* (London: Taylor and Francis)
[21] Ju H L and Sohn H 1997 *J. Magn. Magn. Mater.* **167** 200
[22] Chiorescu C, Neumeier J J and Cohn J L 2006 *Phys. Rev.* B **73** 014406
[23] Volkova N *et al* 2007 *J. Magn. Magn. Mater.* **309** 1
[24] Wagner C, Riggs W, Davis L and Moulder J 1979 *Handbook of X-ray Photoelectron Spectroscopy* ed G E Muilenberg (Eden Prairie, MN: Perkin Elmer Corporation)
[25] Mitchell P C H, Scott C E, Bonnelle J P and Grimblot J G 1987 *J. Catal.* **107** 482
[26] Nagai M, Koizumi K and Omi S 1997 *Catal. Today* **35** 393
[27] Hwang H Y, Cheong S-W, Ong N P and Batlogg B 1995 *Phys. Rev. Lett.* **77** 2041
[28] Wang Z H, Cai J W, Shen B G, Chen X and Zhan W S 2000 *J. Phys.: Condens. Matter* **12** 601
[29] Gayathri N *et al* 1997 *Phys. Rev.* B **56** 1345